

Formation pathway of Population III coalescing binary black holes through stable mass transfer

Kohei Inayoshi^{1*} †, Ryosuke Hirai², Tomoya Kinugawa³ and Kenta Hotokezaka⁴

¹*Department of Astronomy, Columbia University, 550 W. 120th Street, New York, NY 10027, USA*

²*Advanced Research Institute for Science and Engineering, Waseda University, 3-4-1, Okubo, Shinjuku, Tokyo 169-8555, Japan*

³*Institute for Cosmic Ray Research, The University of Tokyo, Chiba 277-8582, Japan*

⁴*Center for Computational Astrophysics, 162 5th Ave, New York, NY, 10010, USA*

28 March 2017

ABSTRACT

We study the formation of stellar mass binary black holes (BBHs) originating from Population III (PopIII) stars, performing stellar evolution simulations for PopIII binaries with MESA. We find that a significant fraction of PopIII binaries form massive BBHs through stable mass transfer between two stars in a binary, without experiencing common envelope phases. We investigate necessary conditions required for PopIII binaries to form coalescing BBHs with a semi-analytical model calibrated by the stellar evolution simulations. The BBH formation efficiency is estimated for two different initial conditions for PopIII binaries with large and small separations, respectively. Consequently, in both models, $\sim 10\%$ of the total PopIII binaries form BBHs only through stable mass transfer and $\sim 10\%$ of these BBHs merge due to gravitational wave emission within the Hubble time. Furthermore, the chirp mass of merging BBHs has a flat distribution over $15 \lesssim M_{\text{chirp}}/M_{\odot} \lesssim 35$. This formation pathway of PopIII BBHs is presumably robust because stable mass transfer is less uncertain than common envelope evolution, which is the main formation channel for Population II BBHs. We also test the hypothesis that the BBH mergers detected by LIGO originate from PopIII stars using the total number of PopIII stars formed in the early universe as inferred from the optical depth measured by Planck. We conclude that the PopIII BBH formation scenario can explain the mass-weighted merger rate of the LIGO’s O1 events with the maximal PopIII formation efficiency inferred from the Planck measurement, even without BBHs formed by unstable mass transfer or common envelope phases.

Key words: gravitational waves – black hole physics – stars: Population III

1 INTRODUCTION

Advanced LIGO (AdLIGO) has detected sources of gravitational waves (GWs). The sources, GW150914, GW151226 and LVT151012, are inferred to be merging binary black holes (BBHs) with masses of $(36.2^{+5.2}_{-3.8} M_{\odot}, 29.1^{+3.7}_{-4.4} M_{\odot})$, $(14.2^{+8.3}_{-3.7} M_{\odot}, 7.5^{+2.3}_{-2.3} M_{\odot})$ and $(23^{+18}_{-6} M_{\odot}, 13^{+4}_{-5} M_{\odot})$ (Abbott et al. 2016b,d). The origin of such massive and compact BBHs and their formation pathways have been proposed (Abbott et al. 2016e, references therein) through massive binary evolution (e.g. Belczynski et al. 2004; Dominik et al. 2012; Kinugawa et al. 2014; Belczynski et al. 2016b) including rapid rotation and tides (Mandel & de Mink 2016; Marchant et al. 2016), and/or stellar dynamics in a dense

cluster (e.g. Portegies Zwart & McMillan 2000; O’Leary et al. 2016; Rodriguez et al. 2016; Mapelli 2016).

In the isolated-binary scenario, metal-poor stars are generically required to form massive BHs because of inefficient stellar winds and smaller stellar radii. Many authors have investigated formation channels of BBHs via Population II (hereafter, PopII) stars with $Z \lesssim 0.1 Z_{\odot}$ (e.g. Dominik et al. 2012; Belczynski et al. 2016b) and Population III (hereafter PopIII) with $Z \simeq 0$ stars (e.g. Kinugawa et al. 2014, 2016b; Belczynski et al. 2016a). The initial mass function (IMF) of PopII stars is expected to be less top-heavy (Omukai et al. 2005), whereas PopIII stars are thought to be typically as massive as $\sim 10 - 300 M_{\odot}$ (e.g., Hirano et al. 2014) and likely to evolve without losing their masses due to stellar winds (e.g. Baraffe et al. 2001; Inayoshi et al. 2013). These scenarios may be distinguished in the future by the chirp mass distributions (Nakamura et al. 2016),

* E-mail: inayoshi@astro.columbia.edu (KI)

† Simons Society of Fellows, Junior Fellow.

where $M_{\text{chirp}} \equiv (M_1 M_2)^{3/5} / (M_1 + M_2)^{1/5}$ for a BBH with masses of M_1 and M_2 , and stochastic GW backgrounds (Abbott et al. 2016c; Hartwig et al. 2016; Inayoshi et al. 2016; Dvorkin et al. 2016; Nakazato et al. 2016).

In PopII BBH formation from isolated binaries, a significant fraction of the binaries experience unstable mass transfer (MT) during the binary evolution (e.g. Dominik et al. 2012; Belczynski et al. 2016b). The unstable MT makes the orbital separation shrink rapidly, which results in a common envelope (CE) phase (Paczynski 1976; Iben & Livio 1993; Taam & Sandquist 2000; Ivanova et al. 2013, references therein), where one of the stars plunges into the bloated envelope of the companion star and spirals inwards, losing its orbital energy and angular momentum. If the stellar envelope is successfully ejected due to the energy deposit and the spiral-in halts, a close binary system would be formed or else these stars would merge. To form BBHs which can merge within the Hubble time, PopII binaries should experience CE phases because their orbital separations tend to be wider due to mass loss (e.g., stellar winds). Moreover, since PopII giant stars are likely to have convective stellar envelopes, the MT would be unstable. Because of uncertainties about relevant physical processes, however, the final outcome of binaries after unstable MT and CE phases is uncertain (e.g., Ivanova et al. 2013). In population synthesis models, in fact, merging rates of PopII BBHs vary by several orders of magnitude depending on the adopted prescriptions about the MT and CE (Belczynski et al. 2008; Dominik et al. 2012; Belczynski et al. 2016b; Eldridge & Stanway 2016)¹.

The CE phase also may play a crucial role for the PopIII binary evolution. Belczynski et al. (2016a) claimed that most of PopIII massive binaries merge in the CE phase thereby only a small fraction of them evolve to merging BBHs. However, as speculated by Kinugawa et al. (2014), there are PopIII binaries which can form BBHs with a coalescence time less than the Hubble time *through stable MT and without experiencing any CE phases*. This is because PopIII stars with certain masses evolve to compact blue giants with a radiative envelope instead of red giants with a convective envelope (e.g., Marigo et al. 2001; Ekström et al. 2008). The discrepancies between Kinugawa et al. (2014) and Belczynski et al. (2016a) come from the difference in models for PopIII single stellar evolution and their prescription to describe binary evolution during CE phases (e.g., stability conditions for MT and merger criteria in CE phases).

In this work, we address the following questions: (i) what conditions are required for the formation of merging PopIII BBHs to avoid the CE phases and (ii) what fraction of PopIII binaries evolve to merging BBHs without the CE phase. Then we compare the total number of PopIII BBHs required from LIGO’s O1 merger rate with the total mass of the PopIII stars in the Universe derived from other astronomical observations. For this purpose, we study PopIII

binary evolution with stellar evolution calculations. In this paper, for the first time, we perform stellar evolution calculations with a public code MESA (Paxton et al. 2011, 2013, 2015, version 8845) to follow evolution processes of massive PopIII binaries (single stellar evolution, orbital evolution and mass transfer; see §2.1) and formation of BBHs. Applying the results, we make a semi-analytical model to describe those binary processes so that the evolutionary tracks match with the results obtained by the detailed calculations of stellar structure. This method is useful to study statistical properties of forming PopIII BBHs for a wide range of initial conditions, i.e., the masses and the orbital separation.

The rest of this paper is organized as follows. In §2, we describe the methodology of our stellar evolution calculations (§2.1) and semi-analytical model (§2.2). In §3, we show the simulation results and discuss the necessary conditions for formation of PopIII BBHs only via stable MT. We also estimate formation efficiency of PopIII BBHs for two scenarios for initial conditions of PopIII binaries. In §4, we discuss the possibility that coalescing PopIII BBHs can explain all the LIGO sources, consistently with observations in the current status. We give discussions and caveats of our calculations in §6 and summarize the main conclusions of this paper in §7.

2 METHODOLOGY

2.1 Stellar evolution calculations

2.1.1 single star evolution

We consider the evolution of massive PopIII stars in the mass range of $20 \leq M/M_\odot \leq 60$. The stellar structure is calculated with a public code MESA. We briefly describe the setup of the calculations but more details are shown in Paxton et al. (2011, 2013, 2015). We use the mixing length theory to treat convection, with the Schwarzschild criterion and a mixing length parameter 1.6. The effects of mass loss due to stellar winds and pulsations are neglected because they are unlikely to affect the stellar structure for the case of PopIII stars (e.g. Baraffe et al. 2001; Inayoshi et al. 2013). We do not follow evolution of a star beyond central carbon (C) ignition because the C burning phase finishes within a few years, in which the binary properties (mass, separation etc) do not change. Instead, we replace the star with a BH (point gravitational source) of the same mass when the original stellar mass (or the core mass) is massive enough to form a BH. We here set the critical mass to $M \geq 28 M_\odot$ in the zero-age main sequence (ZAMS) phase. (e.g., Kinugawa et al. 2014), where the corresponding core masses are $M_{\text{He(CO)}} \gtrsim 9.3$ (7.6) M_\odot .

Fig. 1 presents the Hertzsprung-Russell (HR) diagram for PopIII stars (solid), whose data are taken from Marigo et al. (2001). Before including the binary interactions, we check that results of single stellar evolution for various masses ($20 \leq M \leq 60 M_\odot$) agree well with those shown in Fig. 1. Massive PopIII stars are generally more compact and hotter than metal-enriched PopII/I stars. This is because PopIII stars contract before reaching the ZAMS phase so that the central temperature increases to $\sim 10^8$ K, where helium (He) burning produces a tiny fraction of carbon and thus sufficient energy by hydrogen (H) burning

¹ Pavlovskii et al. (2017) have pointed out that massive stars with convective envelope could be more unlikely to experience unstable MT and CE than previously expected in PopII BBH formation (e.g. Belczynski et al. 2016b), considering a detailed model (Pavlovskii & Ivanova 2015). Although their model also might allow PopIII binaries to form more BBHs even via CE phase, we do not consider the effect to give a conservative discussion.

due to CN-cycle is generated to support the whole structure (e.g. Omukai & Palla 2003). As a result, the effective temperature is $4 \times 10^4 \lesssim T_{\text{eff}} \lesssim 10^5$ K in the ZAMS phase. For $10 \lesssim M/M_{\odot} \lesssim 100$, the onset of central He-burning occurs soon after hydrogen exhaustion in the core. The evolution stage proceeds with an almost constant luminosity towards lower effective temperature. One remarkable feature is that for $10 \lesssim M \lesssim 60 M_{\odot}$ stars the He-core burning and the subsequent nuclear burning terminates before reaching the Hayashi track ($T_{\text{eff}} \sim 10^{3.7}$ K), where stars develop a deep convective envelope (Hayashi 1961; Hayashi et al. 1962). Detailed calculations of stellar structure by other groups (e.g., Ekström et al. 2008) have also shown that a single PopIII star with $M \lesssim 60 M_{\odot}$ is unlikely to have a convective envelope during its lifetime (see their figure 5). Note that properties of the stellar envelope are crucial to determine stability of MT (see §2.1.3).

Recently, Belczynski et al. (2016a) performed population synthesis calculations of PopIII binaries. They describe the time evolution of the stellar radius of PopIII stars, by adopting their lowest metallicity model ($Z = 0.0001$) and assuming that deep convective envelopes are developed even with higher values of T_{eff} depending on stellar masses, e.g., the effective temperatures below which a convective envelope develops are assumed to be $10^{4.4}$ and $10^{4.3}$ K for $M = 20$ and $50 M_{\odot}$, respectively. These correspond to the evolutionary stages when the core helium burning begins. Under such an assumption, MT always results in the CE phase and the outcome is a stellar merger. However, stellar evolution calculations show that PopIII stars do not have convective envelopes at $T_{\text{eff}} > 10^{3.7-3.8}$ K (e.g., Ekström et al. 2008; Hosokawa et al. 2012), that is satisfied at any stage of the late-time evolution of PopIII stars with masses $< 60 M_{\odot}$ as shown in Fig. 1. Therefore we do not expect that the MT between PopIII stars always leads to the CE phase.

2.1.2 binary orbital evolution

We consider the orbital evolution of a binary system of the primary and secondary star with a mass of M_1 and M_2 , respectively. The time evolution of the orbital separation a is calculated by an ordinary differential equation,

$$\frac{\dot{a}}{a} = \frac{2\dot{J}_{\text{orb}}}{J_{\text{orb}}} - \frac{2\dot{M}_1}{M_1} - \frac{2\dot{M}_2}{M_2} + \frac{\dot{M}}{M}, \quad (1)$$

where J_{orb} is the orbital angular momentum of the binary and $M = M_1 + M_2$ is the total mass. As the binary evolves, the mass and the orbital angular momentum will change due to mass transfer (MT) between the two stars and emission of GWs after they collapse into compact objects. Note that circular orbits ($e = 0$) are assumed for simplicity (but see also Dosopoulou & Kalogera 2016a,b).

For conservative MT, i.e., $\dot{J}_{\text{orb}} = 0$ and $\dot{M} = 0$ ($\dot{M}_1 = -\dot{M}_2 \neq 0$), we obtain

$$\frac{\dot{a}}{a} = -\frac{2\dot{M}_1}{M_1} (1 - q_1), \quad (2)$$

where $q_1 = M_1/M_2$. When the primary star loses its mass ($\dot{M}_1 < 0$), thus the orbital separation shrinks (widens) for $q_1 > 1$ ($q_1 < 1$). As an example of non-conservative MT, we consider that the primary transfers its mass to the secondary ($\dot{M}_1 < 0$), and a fraction β of the transferred mass can

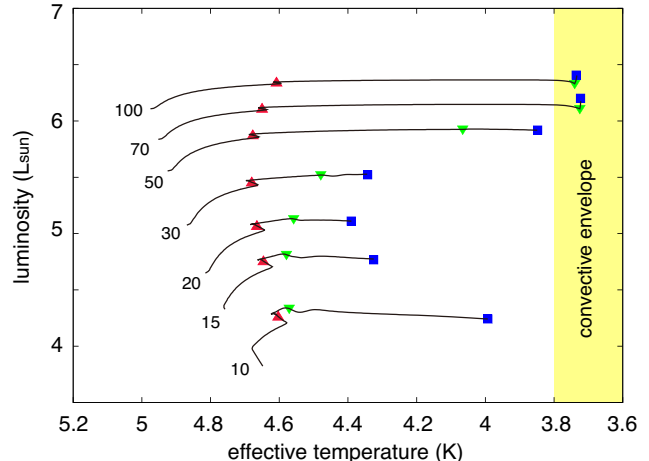


Figure 1. The Hertzsprung-Russell (HR) diagram for PopIII stars with a mass range of $10 \leq M/M_{\odot} \leq 100$ using the data taken from Marigo et al. (2001). Symbols indicate the epochs corresponding to the beginning of the He-core burning (red), the He-shell burning (green) and the C burning (blue), respectively.

accrete on to the secondary and a fraction $(1 - \beta)$ of the mass is lost from the binary system with a specific orbital angular momentum $(M_2/M)^2 \sqrt{GMa}$. Then, the orbital evolution is described as

$$\frac{\dot{a}}{a} = -\frac{2\dot{M}_1}{M_1} \left[1 - q_1 + \frac{q_1(1 - \beta)}{2(1 + q_1)} \right]. \quad (3)$$

This type of non-conservative MT would occur when the accretor, which is fed by gas accretion, is a compact object because the accreted gas onto it releases a huge amount of energy as radiation and/or outflows and a significant fraction of the gas can be ejected (Ohsuga et al. 2005; Jiang et al. 2014; Sądowski et al. 2015).

2.1.3 mass transfer

When one of the stars in a binary exhausts hydrogen at the central core, the star begins to expand. If the Roche lobe around the primary is filled with its bloated envelope, the material is transferred to the secondary star through the first Lagrangian point. The process is the so-called Roche lobe overflow (RLOF). The radius of the Roche lobe (Roche radius) is approximately expressed as (Eggleton 1983):

$$R_{L,1} \simeq a \frac{0.49q_1^{2/3}}{0.6q_1^{2/3} + \ln(1 + q_1^{1/3})}. \quad (4)$$

The behavior of the MT is determined by the response of the Roche radius and the stellar radius when it loses the material (Paczynski 1976). Assuming the MT is conservative ($\beta = 1$), the response of the Roche radius is characterized by

$$\zeta_L \equiv \frac{d \ln R_{L,1}}{d \ln M_1} \simeq 2.13q_1 - 1.67, \quad (5)$$

(Tout et al. 1997). For $\zeta_L < \zeta_*$ ($\equiv d \ln R_1 / d \ln M_1$), the stellar radius shrinks and becomes smaller than the Roche radius after the mass of the primary is transferred. On the other hand, for $\zeta_L > \zeta_*$, the MT would proceed unstably and the two stars would either merge or experience a common envelope (CE) phase. The response of the stellar radius

is automatically calculated in the stellar evolution calculations, while it is estimated with an analytical expression in our semi-analytical model (see §2.2.2).

We adopt the binary module in MESA to treat the MT process. When the Roche radius is filled with stellar material ($R_1 > R_{L,1}$), the mass transfer rate is calculated by a method proposed by Kolb & Ritter (1990),

$$\dot{M}_1 = -2\pi F_1(q_2) \frac{R_{L,1}^3}{GM_1} \times \left[\left(\frac{k_B T_{\text{ph}}}{m_p \mu_{\text{ph}}} \right)^{3/2} \frac{\rho_{\text{ph}}}{\sqrt{e}} + \int_{P_{\text{ph}}}^{P_{L,1}} F_2(\Gamma_1) \left(\frac{k_B T}{m_p \mu} \right)^{1/2} dP, \right] \quad (6)$$

where $F_1(q_2) = 1.23 + 0.5 \log q_2$, $F_2(\Gamma_1) = \Gamma_1^{1/2} [2/(\Gamma_1 + 1)]^{(\Gamma_1+1)/(2\Gamma_1-2)}$, Γ_1 is the first adiabatic exponent, and T_{ph} , μ_{ph} , ρ_{ph} , P_{ph} and $P_{L,1}$ are the temperature, mean molecular weight, density and pressure at the photosphere and the radius of $R_{L,1}$, respectively. The first and second terms correspond to the mass transfer rate for isothermal atmosphere (optically thin) and adiabatic atmosphere (optically thick), respectively. This rate is calculated self-consistently by considering properties of the donor star. Note that conservative mass transfer, i.e. $\dot{J}_{\text{orb}} = 0$ and $\dot{M} = 0$ ($\beta = 1$) is assumed in our stellar evolution calculations.

2.1.4 gravitational wave emission

A binary loses the orbital angular momentum and the energy due to emission of GWs following

$$\frac{\dot{J}_{\text{orb}}}{J_{\text{orb}}} = -\frac{32G^3 M_1 M_2 M}{5c^5 a^4}, \quad (7)$$

where $e = 0$ is assumed. From Eq. (7), the coalescence timescale due to GW emission is estimated as

$$t_{\text{GW}} = \frac{5a^4 c^5}{256G^3 M_1 M_2 M_{\text{tot}}}, \quad \simeq 9.5 \frac{2q_1^2}{1+q_1} \left(\frac{a}{0.2 \text{ AU}} \right)^4 \left(\frac{M_1}{30 M_\odot} \right)^{-3} \text{ Gyr}. \quad (8)$$

2.2 Semi-analytical model

We describe the treatment of PopIII binary stars in our semi-analytical model. The differences from the detailed calculations of stellar structure are shown in the following. Since we do not follow the stellar evolution of binaries, instead we need to treat single stellar evolution (§2.2.1), the MT rate, and the response of the donor and accretor (§2.2.2–2.2.5). The orbital evolution and GW emission from PopIII BBHs are calculated in the same way as in §2.1.2 and 2.1.4.

2.2.1 single star evolution

We adopt fitting formulae for stellar radii and He core mass of PopIII stars with masses of $10 M_\odot \leq M \leq 100 M_\odot$ as functions of the mass and time since the birth of the stars (Kinugawa et al. 2014)². These are based on the results

² The fitting formula for the lifetime in the He-burning and He-shell burning phase were updated (Kinugawa et al. 2016a), which we adopt in this paper.

of the stellar evolution calculations for single PopIII stars by Marigo et al. (2001), where mass loss due to the stellar wind and pulsation are not considered. Note that the time-averaged root-mean-square errors of the fitting formulae are within 6% over the entire lifetime of PopIII stars. We set the critical mass required for BH formation to $M \geq 28 M_\odot$.

2.2.2 stability of mass transfer

In our semi-analytical model, we evaluate stability of MT and estimate the transfer rate, instead of conducting stellar evolution calculations (§2.1). We obtain quantitative criteria for the stability of MT. In summary, PopIII binaries experience unstable MT and CE phases if any of the following conditions are satisfied during the evolution;

- (A) either M_1 or M_2 exceeds $60 M_\odot$,
- (B) $M_2/M_1 \leq 1/3$ at the first MT episode, and
- (C) $\dot{M}_2 > \dot{M}_{\text{crit}} (= 2 \times 10^{-2} M_\odot \text{ yr}^{-1})$.

In what follows, we explain these conditions in more detail.

(A) *Unstable MT due to convective envelope* — The stability of MT is determined by the response of the Roche radius ζ_L and the stellar radius of the donor ζ_* (§2.1.3). In our semi-analytical model, we adopt the analytical expressions for the value of ζ_* as in population synthesis calculations (e.g., Hurley et al. 2002; Belczynski et al. 2008).

At the early stage of the MT, mechanical equilibrium is restored in a dynamical timescale and the star can be assumed to be at hydrostatic equilibrium at every time. That is, the response of the stellar radius occurs adiabatically. The value of $\zeta_{\text{ad}} (\equiv [d \ln R_1 / d \ln M_1]_S)$ depends on whether the stellar envelope is convective or radiative. For a star with a core and a convective envelope, the value of $\zeta_{\text{ad,conv}}$ is expressed as a function of the mass ratio $m_{c,1}$ between the core mass and the total mass in the primary (Hjellming & Webbink 1987; Soberman et al. 1997). The value of $\zeta_{\text{ad,conv}}$ increases with $m_{c,1}$ and approaches $-1/3$ for $m_{c,1} \rightarrow 0$, which corresponds to a fully convective star. As shown in Fig. 1, PopIII stars with $M_1 > 50 M_\odot$ have deep convective envelopes after the onset of He-core burning. From Table 4 of Marigo et al. (2001), $m_{c,1} \simeq 0.45 - 0.5$ for $60 \lesssim M_1/M_\odot \lesssim 100$, respectively. Thus, $\zeta_{\text{ad,conv}} \simeq 0.44 - 0.56$ for the mass range, while $\zeta_L = 2.13q_1 - 1.67 \geq 0.46$ ($q_1 \geq 1$, see Eq. 5). Therefore, PopIII binaries which have components heavier than $60 M_\odot$ are likely to experience unstable MT unless the binary mass ratio is exactly unity or the MT occurs before the donor star reaches the Hayashi track because of a small initial separation. Here, to give a conservative argument, we simply impose that *if either M_1 or M_2 exceeds $60 M_\odot$, the binary does not form a BBH because of unstable MT.*

(B) *Delayed dynamical instability (DDI)* — For a star with a radiative envelope, the value of $\zeta_{\text{ad,rad}}$ is generally positive. When the radiative envelope, which has a positive entropy gradient, is removed by MT, the layer with a lower entropy is exposed. Then, the density will increase to adjust its new hydrostatic equilibrium state with the same external pressure as before because $(\partial S / \partial \rho)_p = -(1/\rho^2)(\partial T / \partial p)_S < 0$. Thus, the donor's radius shrinks

in the dynamical timescale³. However, the situation in this case is more complicated. Even if the MT occurs stably at the early phase ($\zeta_L < \zeta_{ad,rad}$), the inner layer of the donor with a shallower entropy gradient can be exposed. If the entropy profile is shallow enough for the response of the stellar radius to be $\zeta_L > \zeta_{ad,rad}$, the MT would become unstable later due to the so-called delayed dynamical instability (DDI) (Hjellming & Webbink 1987). The critical mass ratio that leads to the DDI has been estimated as $q_{crit,1} = 2 - 4$ for many kinds of donor stars (e.g. Hjellming 1989; Ge et al. 2010; Pavlovskii & Ivanova 2015; Ge et al. 2015). We note that the exact value of the critical mass ratio is still uncertain (e.g. treatment of super-adiabatic layer, see discussions in Pavlovskii & Ivanova 2015), in particular, for metal-poor stars like PopIII stars. We here simply assume $q_{crit,1} = 3$, which is the averaged value for PopI cases. Therefore, we assume that *if the donor star is sufficiently massive ($M_2/M_1 \leq 1/3$), the MT will be unstable due to the DDI*.

(C) *Expansion of accretors due to MT* — The fitting formulae we adopt are obtained by calculations of single stellar evolution, where the stellar structure is thermally relaxed. However, when the first episode of MT occurs, the secondary (main-sequence) star is away from its thermal equilibrium state. In fact, the main-sequence accretor could be bloated, depending on the MT rate. According to detailed stellar evolution calculations by Hosokawa et al. (2016), the accreting PopIII stars are unlikely to expand as long as the accretion rate is $\lesssim 10^{-2} M_\odot \text{ yr}^{-1}$. The critical rate has been also estimated as a few $\times 10^{-2} M_\odot \text{ yr}^{-1}$ (Hosokawa et al. 2012). The exact critical value is still unclear because it depends on treatment of the boundary conditions at the stellar surface. Here, *we adopt the critical accretion rate of $\dot{M}_{crit} \simeq 2 \times 10^{-2} M_\odot \text{ yr}^{-1}$, above which the accretor would expand, fill its Roche lobe and might lead to unstable MT*.

2.2.3 mass transfer rate

In the following, we focus on cases with stable MT in the dynamical timescale ($\zeta_L < \zeta_{ad}$). Even in this case, the donor star gradually approaches its thermal equilibrium state, in which the response of the stellar radius can be satisfied with $\zeta_L > \zeta_{th} \equiv (d \ln R_1 / d \ln M_1)|_{th}$ depending on the stellar structure. When the Roche lobe is filled with the stellar material due to thermal relaxation, MT occurs again in the Kelvin-Helmholtz timescale ($t_{KH} \equiv GM_1^2 / R_1 L_1$). The MT rate is given by the overflowing of the donor's Roche lobe, $\Delta R_1 \equiv R_1 - R_{L,1} (\geq 0)$, as

$$\dot{M}_1 = - \frac{f(\mu) M_1}{\sqrt{R_1^3 / G M_1}} \left(\frac{\Delta R_1}{R_1} \right)^3 d_{3/2}, \quad (9)$$

where

$$f(\mu) = \frac{4\mu\sqrt{\mu}\sqrt{1-\mu}}{(\sqrt{\mu} + \sqrt{1-\mu})^4} \left(\frac{a}{R_1} \right)^3, \quad (10)$$

$\mu = M_1 / (M_1 + M_2)$ and $d_{3/2} = 0.2203$ (e.g. Paczyński & Sienkiewicz 1972; Savonije 1978; Edwards & Pringle 1987).

³ The entropy hardly changes by emitting radiation within a dynamical time since the thermal relaxation timescale of most parts of the envelope is longer than the dynamical timescale.

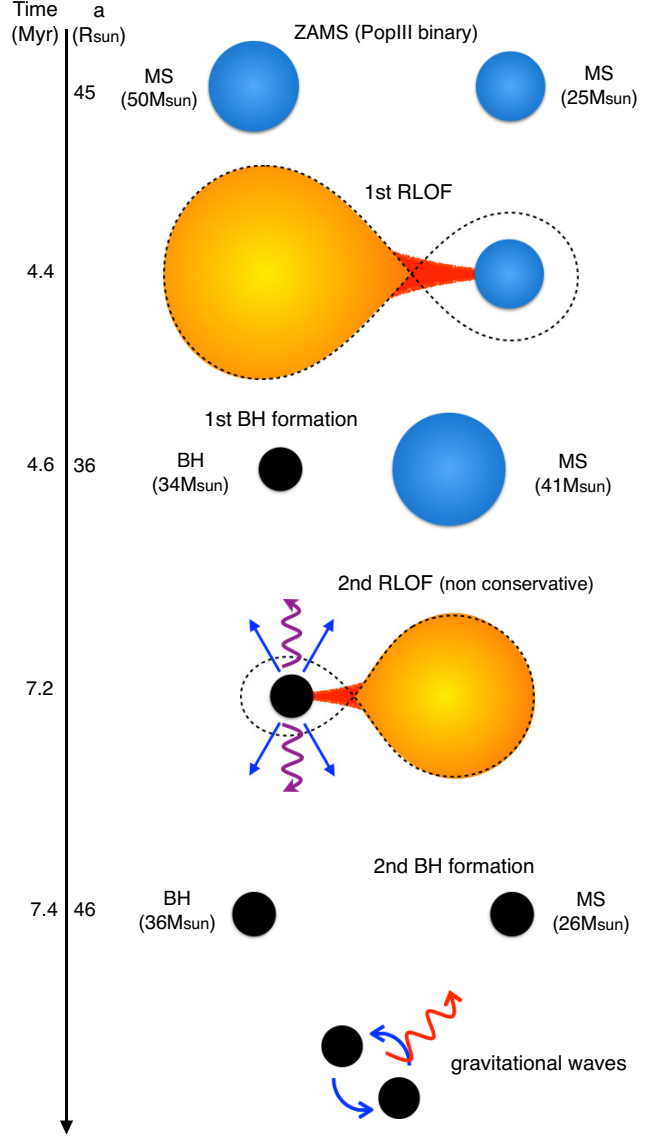


Figure 2. Schematic overview of a typical pathway to form PopIII BBH without experiencing CE phases. The initial conditions are set to $M_{1,0} = 50 M_\odot$, $M_{2,0} = 25 M_\odot$ and $a_0 = 45 R_\odot$.

Note that a polytropic equation of state with an index of $n = 3/2$ is assumed in Eq. (9). In fact, radial dependence of the adiabatic index affects the MT rate (see e.g., Kolb & Ritter 1990; Ge et al. 2010). However, we here adopt the simpler prescription because our semi-analytical model has a lack of thermal properties of the donor's envelope.

The MT rate in Eq.(9) is high soon after the onset of the MT. However, the MT proceeds in the KH timescale of the donor star. Thus, we set the maximum MT rate to $\dot{M}_{1,max} = M_1 / t_{KH,1}$. Typically, $t_{KH,1} \simeq 4 \times 10^3 \text{ yr} (M_1 / 50 M_\odot)^2 (R_1 / 20 R_\odot)^{-1} (L_1 / 10^6 L_\odot)^{-1}$ and then $\dot{M}_{1,max} \simeq 1.25 \times 10^{-2} M_\odot \text{ yr}^{-1}$. To estimate the KH timescale, we adopt a fitting form of the stellar luminosity at the beginning of He-shell burning phase given by Kinugawa et al. (2014). In fact, since the stellar luminosity of the donor rapidly decreases during the MT (Paczynski 1967), we underestimate the value of $t_{KH,1}$ and overestimate the

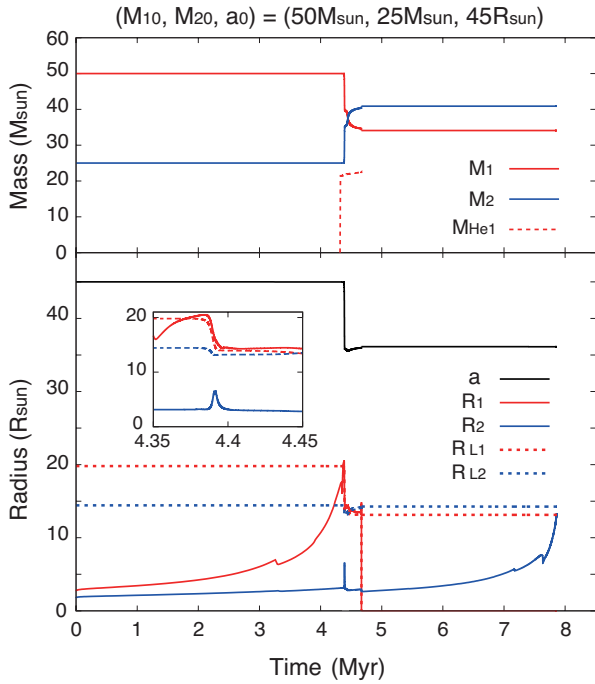


Figure 3. *Top:* Time evolution of stellar masses of a PopIII binary obtained by stellar evolution calculation with MESA. The initial conditions are set to $M_{1,0} = 50 M_{\odot}$, $M_{2,0} = 25 M_{\odot}$ and $a_0 = 45 R_{\odot}$. The primary (red) and secondary (blue) mass and the He core mass of the primary star (red dashed) are shown. *Bottom:* Time evolution of stellar radii (red and blue solid) and the orbital separation (black solid) of the same binary as in the top panel. The Roche radii of the two stars are shown by dashed curves. After the MT, the binary properties change to $M_1 = 34 M_{\odot}$, $M_2 = 41 M_{\odot}$, $M_{\text{He},1} = 22 M_{\odot}$ and $a = 36 R_{\odot}$. We set the He core mass to zero after the star collapses into a BH.

maximum accretion rate. In other words, the condition (C) in §2.2.2 would be alleviated somewhat in detailed stellar evolution calculations.

2.2.4 stellar radii during MT and rejuvenation

During a MT episode, the donor’s radius changes depending on how much of the mass is removed from the envelope. This process is generally complicated and difficult to be treated properly. For simplicity, we consider cases where the donor star is a giant in which He burning begins and the accretor is a main-sequence star. Note that MT between two main-sequence stars (the so-called case A) is not considered to avoid complicated situations.

The stellar radius of the donor during the MT is estimated using the fitting formulae for single star models as $R_1(M_1, t, t_i(M_1)) \rightarrow R_1(M_1 + \delta M_1, t + \delta t, t_i(M_1))$, where δt is the time after the onset of the MT, $\delta M_1 = \int_0^{\delta t} \dot{M}_1 dt (< 0)$ and $t_i(M_1)$ is the lifetime during He core ($i = \text{He}$) and He-shell ($i = \text{HeS}$) burning phases. This prescription assumes that the core mass and the stellar age in the corresponding phase does not change during the MT because the MT occurs faster than the nuclear core and/or shell burning (see also the results with MESA shown in Figs. 3 and 4).

The accretor is fed at a rate of $\dot{M}_2 (= -\dot{M}_1 > 0)$. Since

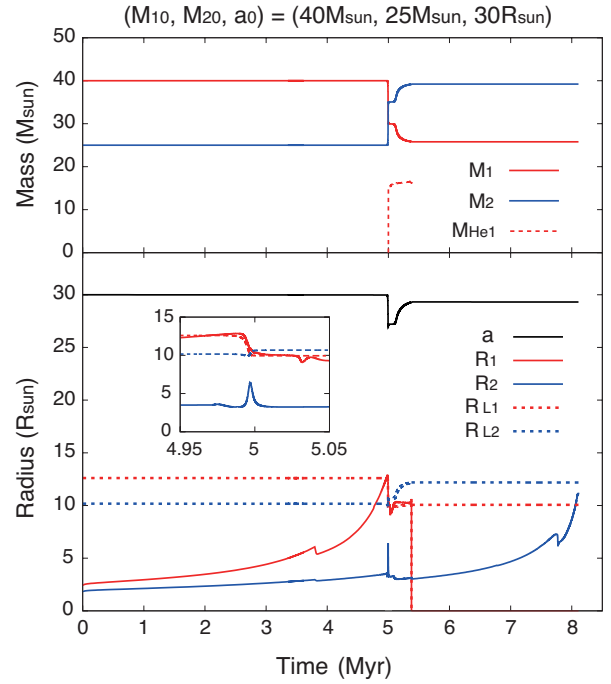


Figure 4. Same as Fig. 3, but different initial conditions of the binary; $M_{1,0} = 40 M_{\odot}$, $M_{2,0} = 25 M_{\odot}$ and $a_0 = 30 R_{\odot}$. After the MT, the binary properties change to $M_1 = 26 M_{\odot}$, $M_2 = 40 M_{\odot}$, $M_{\text{He},1} = 16 M_{\odot}$ and $a = 29 R_{\odot}$.

unburnt hydrogen is supplied as fuel, we modify the stellar age (i.e. rejuvenation) following a method suggested by Tout et al. (1997) and Hurley et al. (2002). We approximate that the mass of H-burning core is proportional to $M_2 \cdot t / t_{\text{H}}(M_2)$, where t is the stellar age. Thus, we estimate a new stellar age due to rejuvenation as

$$t' = \frac{M_2}{M_2 + \delta M_2} \frac{t_{\text{H}}(M_2 + \delta M_2)}{t_{\text{H}}(M_2)} t. \quad (11)$$

Using Eq. (11), we estimate the stellar radius of the accretor as $R_2(M_2 + \delta M_2, t', t_{\text{H}}(M_2 + \delta M_2))$.

2.2.5 termination of MT

The episode of MT terminates at the end of lifetime of the donor or when a large fraction of its hydrogen envelope is stripped from the donor. In the latter case, the donor’s radius rapidly shrinks when the He core mass dominates its total mass. Note that we define the core boundary as the outermost part where the H mass fraction is lower than 0.01 and the He mass fraction is higher than 0.1. The critical ratio of the He core to the total mass is supposed to be $q_{\text{He,crit}} \simeq 0.6 - 0.8$, above which the donor star evolves blueward in the HR diagram (Kippenhahn & Weigert 1990). In our semi-analytical model, we set $q_{\text{He,crit}} \simeq 0.58$ so that the evolutionary tracks of the PopIII binaries agree with the results by the stellar evolution calculations.

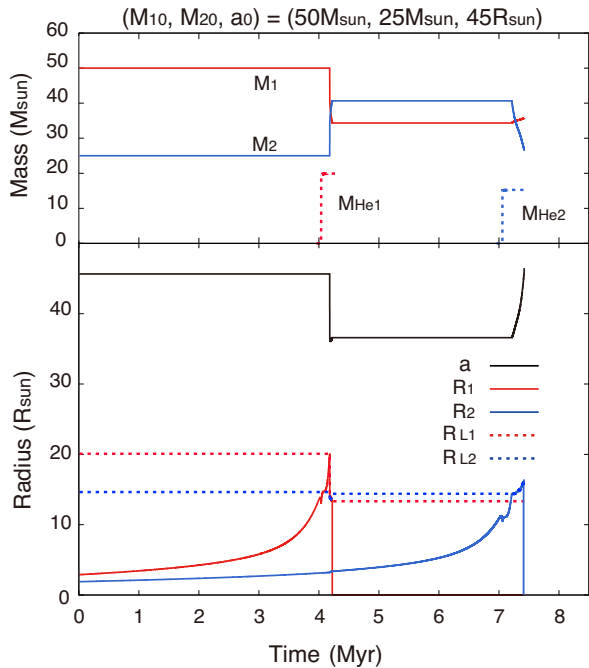


Figure 5. Time evolution of stellar masses, stellar radii, and the orbital separation of a PopIII binary calculated by the semi-analytical model. The initial conditions are set to $M_{1,0} = 50 M_{\odot}$, $M_{2,0} = 25 M_{\odot}$ and $a_0 = 45 R_{\odot}$, which are the same as in Fig. 3.

3 POPULATION III BINARY BH FORMATION

In this section, we discuss the evolutionary paths of PopIII binaries. As an example, Fig. 2 shows a schematic picture of the time evolution of a PopIII binary with the initial masses of $M_{1,0} = 50 M_{\odot}$ and $M_{2,0} = 25 M_{\odot}$ and the initial separation of $a_0 = 45 R_{\odot}$. This is a typical pathway of formation of PopIII BBHs without unstable MT and CE phases. In what follows, we first demonstrate two cases of binary evolution pathways calculated with MESA. Then, we compare these results with the semi-analytic formulae developed in the previous section.

3.1 Evolution of individual PopIII binaries

3.1.1 stellar evolution calculations

We present the time evolution of two PopIII binaries with different initial conditions of $(M_{1,0}, M_{2,0}, a_0) = (50 M_{\odot}, 25 M_{\odot}, 45 R_{\odot})$ in Fig. 3 and $(M_{1,0}, M_{2,0}, a_0) = (40 M_{\odot}, 25 M_{\odot}, 30 R_{\odot})$ in Fig. 4, respectively. Red and blue curves show the evolution of the primary and secondary star, respectively. In each figure, the top panel shows the mass evolution of the two stars $M_{1(2)}$ (solid) and the He core of the primary star $M_{\text{He},1}$ (dashed), and the bottom panel shows the evolution of the stellar radii $R_{1(2)}$ (solid), the Roche radii $R_{L,1(2)}$ (dashed) and the orbital separation a (black solid). Note that these results shown in Figs. 3 and 4 are obtained by stellar evolution calculations with MESA. We follow the evolution of these binaries until just before the second episode of MT occurs because the MT (from the secondary star to a BH) is not conservative. Instead, the non-conservative MT is studied with our semi-analytical model,

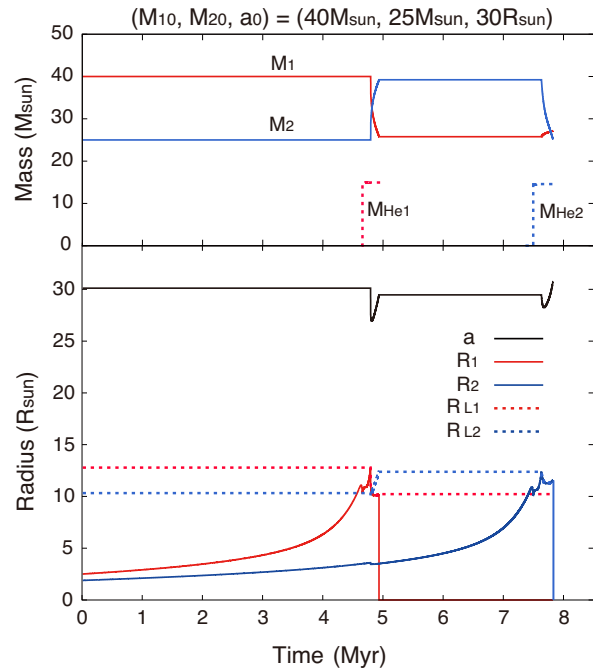


Figure 6. Same as Fig. 5 (semi-analytical model), but different initial conditions of the binary; $M_{1,0} = 40 M_{\odot}$, $M_{2,0} = 25 M_{\odot}$ and $a_0 = 30 R_{\odot}$, which are the same as in Fig. 4.

exploring the dependence of the results on the parameter β (see Appendix A).

As shown in Fig. 3, after the two stars evolve from their ZAMS to post-main-sequence phases, their stellar radii expand. The primary star fills its Roche lobe after the end of the H-core burning and the first episode of MT begins at $t \simeq 4.39$ Myr. Since the mass ratio at the onset of the MT is larger than unity ($q_1 > 1$) and the MT is conservative ($\dot{M}_1 = -\dot{M}_2 > 0$), the separation initially shrinks (see Eq. 2). After the mass ratio becomes smaller than unity, the MT continues and thus the separation gets wider. Once the hydrogen rich layer of the envelope is removed, the MT terminates at $t \simeq 4.6$ Myr due to the discrete change in the surface composition. This occurs just beneath the outermost convection zone in the hydrogen shell, where the helium abundance increases by a factor of ~ 2 . By this time, the He core mass occupies $\sim 65\%$ of the total mass. The core mass of $\simeq 22 M_{\odot}$ is massive enough to form a BH by direct collapse. Note that we do not calculate the evolution of the (primary) naked He star but the primary star is considered as a BH with $M_1 \simeq 22 M_{\odot}$ because of the absence of the wind-mass loss.

During the first episode of MT, the mass of the secondary star is increased to $\simeq 41 M_{\odot}$. The maximum MT rate is $\simeq 2 \times 10^{-3} M_{\odot} \text{ yr}^{-1}$ at the early stage and drops to $\lesssim 10^{-5} M_{\odot} \text{ yr}^{-1}$ later. After the MT, the secondary star becomes massive enough to form a BH.

The overall behaviors for the two cases shown in Figs. 4 and 3 are similar. For both cases, the first episodes of MT terminate when the He-core mass of the primary stars occupies 65 (62)% of their total mass.

3.1.2 semi-analytical model

In Figs. 5 and 6, we show the time evolution of two PopIII binaries calculated by the semi-analytical model. The same initial conditions are adopted for both cases as in Figs. 3 and 4. The evolutionary tracks until just before the second episodes of MT are very similar to those of the stellar evolution calculations. Note that our semi-analytical model does not replicate expansion phases of the secondary stars during the first episodes of MT as shown in Figs. 3 and 4. Here, the critical core mass ratio is set to be $q_{\text{He,crit}} = 0.58$ in order to determine the termination of the MT. This value is slightly smaller than the actual values estimated in §3.1.1, but allows us to reproduce the plausible results by our simple model.

In the second episode of MT, the donor is an ordinary star but the accretor is a BH. Since the MT rate is estimated as $|\dot{M}_2| \sim 10^{-5} - 10^{-3} M_{\odot} \text{ yr}^{-1}$, the BH is fed at a super-Eddington accretion rate of $|\dot{M}_2|/\dot{M}_{\text{Edd},1} \simeq O(10 - 10^3)$, where $\dot{M}_{\text{Edd},1} \equiv L_{\text{Edd},1}/(\epsilon c^2) \simeq 6.9 \times 10^{-7} M_{\odot} \text{ yr}^{-1} (M_1/30 M_{\odot})(\epsilon/0.1)^{-1}$, $L_{\text{Edd},1}$ is the Eddington luminosity and ϵ is the radiative efficiency. Although one assumes that the accretion rate is limited by the Eddington accretion, i.e. $\dot{M}_1 = \min(|\dot{M}_2|, \dot{M}_{\text{Edd},1})$, super(hyper)-Eddington accretion would be possible through an optically-thick accretion disk associated with outflows and/or jets (e.g. Begelman 1978; Abramowicz et al. 1988; Ohsuga et al. 2005; Jiang et al. 2014; Sądowski et al. 2015). We simply assume that a fraction $\beta = \dot{M}_1/|\dot{M}_2| = 0.1$ of the gas can accrete onto the BH and the rest is ejected from the BH with a certain specific angular momentum. We follow the orbital evolution using Eq. (3). Finally, the stellar envelope of the secondary star is stripped and the second episode of MT terminates. The secondary (naked He star) collapses into a BH and thus a binary BH system forms.

3.2 Parameter dependence on final states of PopIII binaries

Fig. 7 shows final fates of PopIII massive binaries with different initial conditions of $q_{2,0} = M_{2,0}/M_{1,0}$ and a_0 for three different primary masses of $M_{1,0} = 30$ (top), 40 (middle) and 50 M_{\odot} (bottom), respectively. Shaded regions indicate initial conditions for which massive PopIII binaries form BBHs (blue), form NS-BH binaries (green) and experience CE phases due to unstable MT (red). With larger initial separations, stellar radii of the two stars never exceed their Roche radii, and they do not interact through MT, indicated as “No RLOF”, where each of the stars evolve as a single star. Dashed lines show boundaries, in the right-hand side of which the binary can form a wide-separation BBH even without binary interactions. It is worthy noting that such wide-separation BBHs formed in “No RLOF” do not merge within the Hubble time. On the other hand, with very small separations, the primary star fills its Roche radius even during its main-sequence phase (the so-called case A mass transfer). In this case, episodes of MT would be likely to affect the evolution of the core mass because the core evolution has not been decoupled yet from that of the total mass. Thus, our treatment for the stellar evolution and its rejuvenation would not work. In addition, the effects due to tidal force could be important for such close binaries (see §6.2).

In the top panel, the parameter dependence of the final

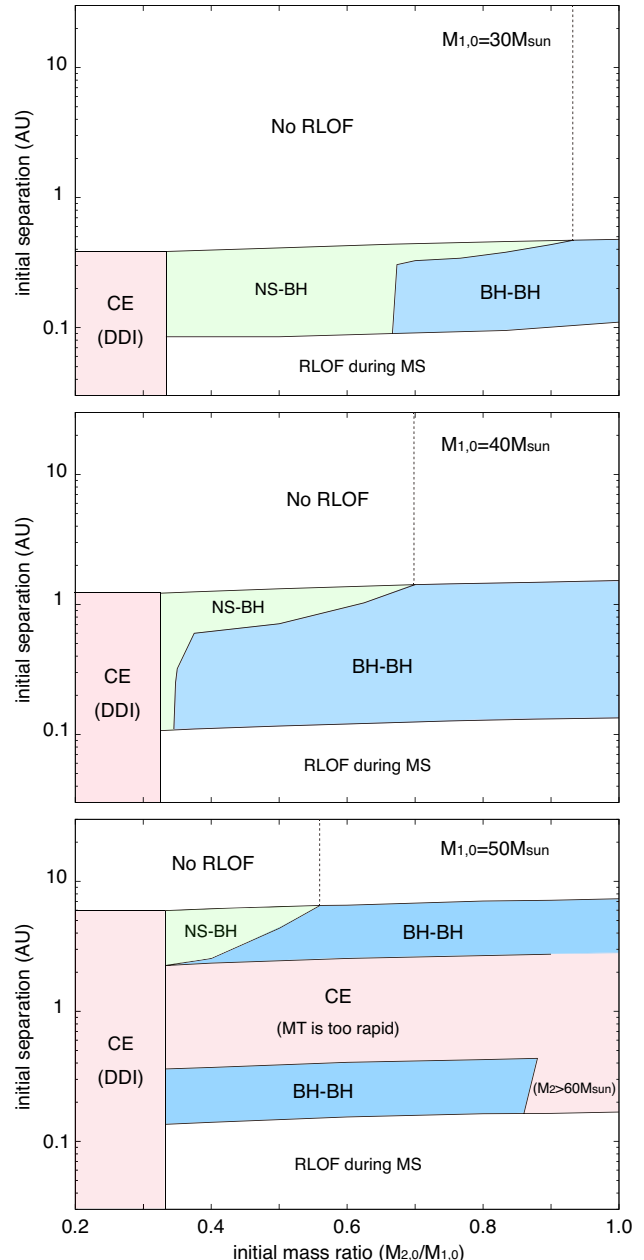


Figure 7. Dependence of final states of PopIII binaries on the initial conditions of the mass ratio $q_{2,0} (= M_{2,0}/M_{1,0})$ and the orbital separation a_0 . Shaded regions indicate conditions for which BBHs form (blue), NS-BH form (green) and PopIII binaries experience CE phases (red). For $q_{2,0} \leq 1/3$, the binaries experience the delayed dynamical instability (DDI). For $M_{1,0} = 50 M_{\odot}$, the binaries are likely to experience CE phases during either the first or second episode of MT.

fates of PopIII binaries with $M_{1,0} = 30 M_{\odot}$ is shown. With smaller mass ratio of $q_{2,0} = M_{2,0}/M_{1,0} \leq 1/3$, the MT is unstable by the DDI (see §2.2.2) and thus the binary plunges into a CE phase. For other cases, compact binaries (BBH or NS-BH) are formed as remnants only via stable MTs. Even for an initially less massive star, its mass can increase via MT to $\gtrsim M_{\text{crit,BH}} (\sim 28 M_{\odot})$, above which the star collapses directly into a BH without explosions. In other words, the

MT from the massive primary allows the secondary to be massive enough to form a BH. For higher initial primary mass ($M_{1,0} = 40 M_{\odot}$), the overall result is similar to that for $M_{1,0} = 30 M_{\odot}$, but BBHs can form for a wider range of initial conditions of binaries.

For the highest primary mass ($M_{1,0} = 50 M_{\odot}$), the PopIII binary is more likely to experience CE phases for the two reasons described in §2.2.2. One is that the secondary star becomes more massive than $\simeq 60 M_{\odot}$ via the first episode of MT. Thus, when the secondary star fills its Roche lobe and undergoes the second episode of MT, the MT is unstable because its stellar envelope is convective. Another reason is that the MT rate from the primary to the secondary can be higher than the critical value of $\dot{M}_{\text{crit},2}$, above which the secondary stellar radius would be bloated. As a result, in this case ($M_{1,0} = 50 M_{\odot}$), PopIII binaries with smaller (~ 0.2 AU) or larger (~ 4 AU) separations can form BBHs via stable MT without experiencing CE phases.

In summary, we find that there are regions in the parameter space where merging BBHs are formed from PopIII binaries without experiencing CE phases. We consider these pathways are robust to form PopIII merging BBHs. In the following discussion, we focus only on such a population because the outcome of the CE phases of PopIII binaries is uncertain. In this sense, our argument on the event rate of BBH mergers is somewhat conservative.

4 FORMATION EFFICIENCY AND POPULATION OF POPIII BINARY BHS

In the previous section, we discussed formation pathways of PopIII BBHs, in particular, focusing on those with or without unstable MT and CE phases. Applying the results, we estimate efficiency of PopIII BBH formation for given initial conditions of PopIII binaries. In the following, we discuss the BBH formation efficiency with an analytical argument in §4.1. As we will see, this estimate gives reasonable BBH formation efficiencies and the delay time distribution. We also build population synthesis models for two types of binary initial conditions as examples (see §4.2 and 4.3). The initial conditions of N_{tot} binaries are generated with the Monte Carlo method and then the evolution is followed by the semi-analytic formula developed in §2.2. The convergence of the results has been checked for $N_{\text{tot}} = 10^5$ and 10^6 . Note that we focus only on PopIII BBH formation through stable MT, i.e., without experiencing any case A MT and CE phases. If BBHs formed via these processes, the efficiency of BBH formation could be higher.

4.1 Analytical estimate

Here we estimate analytically the number fraction of PopIII BBHs coalescing within the Hubble time to the total number of PopIII binaries, $f_{\text{BBH}} = I/J$, where

$$I = \int_{M_{\text{crit},1}}^{M_{\text{crit},2}} dM_1 \Psi(M_1) \int_{q_{\text{crit}}}^1 dq \Phi(q) \int_{a_{\text{crit}}}^{a_{\text{GW}}} da \Gamma(a), \quad (12)$$

and

$$J = \int_{M_{\text{min}}}^{M_{\text{max}}} dM_1 \Psi(M_1) \int_{q_{\text{min}}}^1 dq \Phi(q) \int_{a_{\text{min}}}^{a_{\text{max}}} da \Gamma(a). \quad (13)$$

Here $\Psi(M_1)$ is the IMF for the primary star with $M_{\text{min}} \leq M_1 \leq M_{\text{max}}$, $\Phi(q)$ is the initial mass-ratio distribution with $q_{\text{min}} (= M_{\text{min}}/M_1) \leq q \leq 1$, $\Gamma(a)$ is the initial distribution of binary separations with $a_{\text{min}} \leq a \leq a_{\text{max}}$. For a primary star with $M_1 > M_{\text{crit},1}$, it forms a BH by direct collapse. For $M_1 > M_{\text{crit},2}$, the primary evolves a red giant with a deep convective envelope, resulting in unstable MT and a CE phase (see §2.2.2). We here set $M_{\text{crit},1} = 28 M_{\odot}$ and $M_{\text{crit},2} = 60 M_{\odot}$, respectively. We define $q_{\text{crit}} = \max(q_{\text{min}}, q_{\text{CE}})$, where $q_{\text{CE}} = 1/3$ is the critical mass ratio below which a binary could evolve through a CE phase due to the delayed dynamical instability. As shown in §3.1.2 (Figs. 5 and 6), the orbital separation after forming a BBH hardly changes from the initial separation. The critical separation for a formed BBH required to merge within the Hubble time is estimated as $a_{\text{GW}} \simeq 0.22 \text{ AU} (M_1/30 M_{\odot})^{3/4}$, where formed BBHs are assumed to be equal-mass binaries (see Figs 5 and 6). The value of $a_{\text{crit}} (\simeq 0.1 \text{ AU})$ is adopted so that PopIII binaries do not experience (case A) MT during their main-sequence phases (see Fig. 7). As long as $\Gamma(a)$ is not a steep function at $0.1 \lesssim a/\text{AU} \lesssim 0.3$, therefore, Eq. (12) can be approximated as

$$I \simeq \int_{a_{\text{crit},0}}^{a_{\text{GW},0}} da \Gamma(a) \times \int_{M_{\text{crit},1}}^{M_{\text{crit},2}} dM_1 \Psi(M_1) \int_{q_{\text{crit}}}^1 dq \Phi(q), \quad (14)$$

where $a_{\text{GW},0} = 0.22 \text{ AU}$ and $a_{\text{crit},0} = 0.1 \text{ AU}$. Using Eqs. (13) and (14), and assuming $\Gamma(a) \propto a^{\gamma}$, we can estimate

$$f_{\text{BBH}} \simeq \frac{\int_{M_{\text{crit},1}}^{M_{\text{crit},2}} dM_1 \Psi(M_1) \int_{q_{\text{crit}}}^1 dq \Phi(q)}{\int_{M_{\text{min}}}^{M_{\text{max}}} dM_1 \Psi(M_1) \int_{q_{\text{min}}}^1 dq \Phi(q)} \times \begin{cases} \frac{\ln(a_{\text{GW},0}/a_{\text{crit},0})}{\ln(a_{\text{max}}/a_{\text{min}})} & (\gamma = -1), \\ \frac{(a_{\text{GW},0}^{\gamma+1} - a_{\text{crit},0}^{\gamma+1})}{(a_{\text{max}}^{\gamma+1} - a_{\text{min}}^{\gamma+1})} & (\gamma \neq -1). \end{cases} \quad (15)$$

In addition, we can estimate the number of PopIII BBHs which merge in coalescence timescales of t_{GW} as

$$\frac{dN}{dt_{\text{GW}}} = \frac{dN}{da} \frac{da}{dt_{\text{GW}}} \simeq \Gamma(a) \frac{a}{t_{\text{GW}}} \propto t_{\text{GW}}^{(\gamma-3)/4}, \quad (16)$$

where we use $dN/da \simeq \Gamma(a) \propto a^{\gamma}$ and $t_{\text{GW}} \propto a^4$ (see Eq. 8). Note that the coalescence time distribution is not sensitive to the choice of γ .

It is worthy estimating the efficiency of BBH formation which allows pathways even through unstable MT and CE phases. The efficiency can be roughly estimated as $f_{\text{BBH,max}} = K/J$, where

$$K \simeq \int_{a_{\text{crit},0}}^{a_{*,0}} da \Gamma(a) \times \int_{M_{\text{crit},1}}^{M_{\text{max}}} dM_1 \Psi(M_1) \int_{q_{\text{min}}}^1 dq \Phi(q). \quad (17)$$

Here, the conditions (A) and (B) shown in §2.2.2 are removed, i.e., $M_{\text{crit},2} \rightarrow M_{\text{max}}$ and $q_{\text{crit}} \rightarrow q_{\text{min}}$. We also allow rapid MT to form BBHs (see condition C in §2.2.2) and thus set $a_{*,0} \simeq 1 \text{ AU}$ (see bottom panel in Fig. 7).

4.2 Two types of binary initial conditions

PopIII binaries would form due to fragmentation in a circumstellar disk at $\sim 1 - 100 \text{ AU}$ (Machida et al. 2008; Clark et al. 2011; Greif et al. 2012; Hosokawa et al. 2016) and/or at larger scales of $\sim 10^3 \text{ AU}$ (Turk et al. 2009; Stacy & Bromm

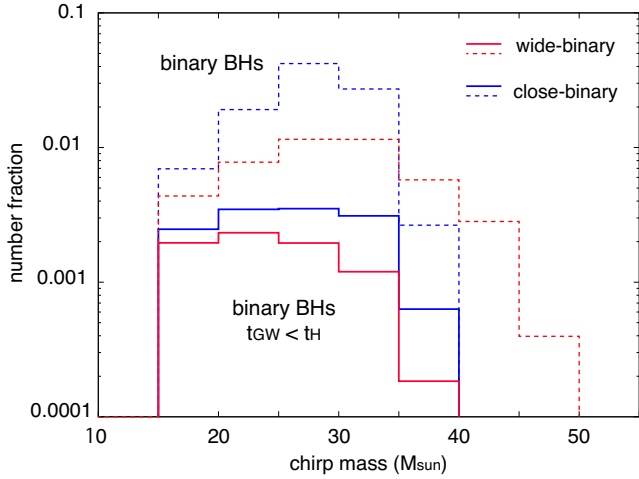


Figure 8. Chirp mass distribution of PopIII BBHs for the wide-binary (red) and close-binary (blue) model, respectively. PopIII BBHs formed through stable MT (dashed) and PopIII BBHs coalescing within the cosmic age, $t_{\text{GW}} < 13.8$ Gyr (solid) are shown.

2013). In addition, massive PopIII stars emit strong UV radiation (Hosokawa et al. 2011; Stacy et al. 2012), which affects gas accretion onto the proto-binary and the final masses. Susa et al. (2014) have studied statistical properties of PopIII binaries in ~ 60 mini-halos, performing radiation hydrodynamical simulations with a spatial resolution of ~ 10 AU. As a result, the binary fraction is $\sim 50\%$ and the separation is $10 - 10^3$ AU. Stacy et al. (2016) have performed a cosmological simulation including radiative feedback with a very high-resolution of ~ 1 AU. They studied star formation in one mini-halo and found that a close massive PopIII binary forms with $13 + 15 M_{\odot}$ and $a \sim 5$ AU.

4.2.1 wide-binary model

As an example, we consider the same initial conditions as in Kinugawa et al. (2014), where a classical model for initial conditions of field binaries (e.g., Hurley et al. 2002) is applied for PopIII binaries. Namely, we adopt a flat IMF, $\Psi(M_1) \propto \text{const.}$, for the primary star with $10 \leq M_1/M_{\odot} \leq 100$, a flat mass-ratio distribution, $\Phi(q) \propto \text{const.}$, with $q_{\text{min}} (= 10 M_{\odot}/M_1) \leq q \leq 1$, and a log-flat distribution for the orbital separation, $\Gamma(a) \propto a^{-1}$. The minimum separation is set so that the binary does not fill its Roche radius from the beginning. We set $a_{\text{max}} = 10^6 R_{\odot} (\simeq 4.6 \times 10^3 \text{ AU})$. In this model, the number fraction of PopIII BBHs formed by stable MT is estimated from Eq. (15) as

$$f_{\text{BBH}} \simeq \frac{\ln\left(\frac{a_{\text{GW},0}}{a_{\text{crit},0}}\right)}{\ln\left(\frac{a_{\text{max}}}{a_{\text{min}}}\right)} \times \frac{\frac{2}{3}(M_{\text{crit},2} - M_{\text{crit},1})}{M_{\text{max}} - M_{\text{min}}[1 + \ln(\frac{M_{\text{max}}}{M_{\text{min}}})]}. \quad (18)$$

Note that this equation is valid for $M_{\text{min}} \leq M_{\text{crit},1}/3 \simeq 9.3 M_{\odot}$. Adopting the values of the initial conditions, we estimate as $f_{\text{BBH}} \simeq 0.02$ from Eq. (18), where we adopt $a_{\text{min}} \simeq 3R_1 \simeq 7 R_{\odot}$. In this condition, adding to $f_{\text{BBH}} \simeq 0.02$ the possibility that BBHs are also formed by unstable MT, Eq.

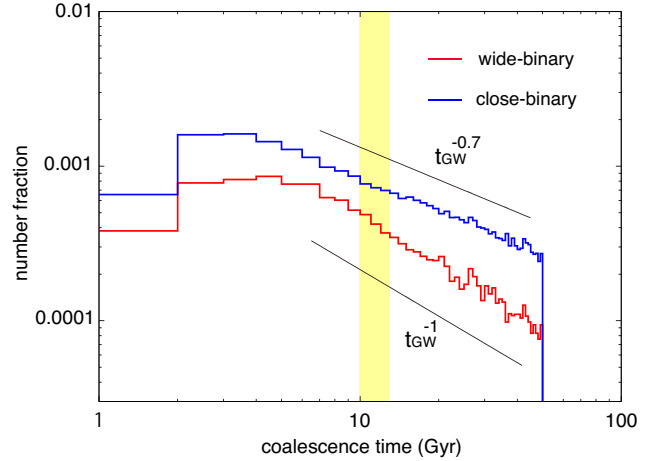


Figure 9. Distribution of the coalescence time of PopIII BBHs for the wide-binary (red) and close-binary (blue) model, respectively. Shaded region shows PopIII BBHs which can merge within the LIGO detection horizon.

(17) gives a maximum formation efficiency $f_{\text{BBH,max}} \sim 0.1$, which is consistent with that by Kinugawa et al. (2014).

4.2.2 close-binary model

Different initial conditions have been suggested by Belczynski et al. (2016a) for close Pop III binaries (close-binary model). These initial conditions are motivated by N-body simulations by Ryu et al. (2016), who follow the time evolution of multiple systems in a star-forming cloud in a mini-halo. They considered that PopIII stars form due to disk fragmentation around $10 - 20$ AU and these stars lose their angular momentum by dynamical friction with the ambient gas, resulting in formation of stable close binaries⁴. The distribution of the initial separation is given by a Gaussian function with the average of $\langle a \rangle \simeq 0.4$ AU and the dispersion of $\sigma_a \simeq 0.34$ AU. The primary mass and the mass ratio in this model have bimodal distributions, respectively (see Table 2 of Belczynski et al. 2016a in detail).

4.3 Resultant distribution functions

Fig. 8 presents the chirp-mass distribution of PopIII BBHs for the wide-binary (red) and close-binary (blue) model, respectively. Note that the chirp mass is a physical quantity to determine the leading-order amplitude and frequency evolution of the GW signal. The values of y-axis is normalized by the total number of PopIII binaries N_{tot} ; PopIII BBHs formed through stable MT (dashed) and PopIII BBHs coalescing within the cosmic age, $t_{\text{GW}} < 13.8$ Gyr (solid). For the wide-binary model, 0.8% of the PopIII binaries form

⁴ Ryu et al. (2016) assumed a uniform density distribution of the ambient gas ($n_{\text{gas}} = 10^6 \text{ cm}^{-3}$) at $10 - 20$ AU, and neglected radiative feedback. Since the gas density at such small scales is $> 10^{14} \text{ cm}^{-3}$ (Greif et al. 2012), however, the effect of dynamical friction would be underestimated. Moreover, radiation from the formed binaries would determine their final properties as shown in Stacy et al. (2016).

BBHs through stable MT and can merge due to GW emission within the Hubble time. This result is consistent with the analytical estimate of the fraction shown in §4.1, where $f_{\text{BBH}} \simeq 2\%$ is estimated. This difference is due to the simplification in Eq. (15). In fact, PopIII BBHs with high chirp masses $35 \lesssim M_{\text{chirp}}/M_{\odot} \lesssim 45$ are formed, but do not merge because of their large separations (see also bottom panel in Fig. 7). On the other hand, for the close-binary model, 1.3% of the PopIII binaries form BBHs through stable MT and can merge due to GW emission within the Hubble time. In this model, the initial-separation distribution has a peak at $a_0 \simeq 100 R_{\odot} (\simeq 0.5 \text{ AU})$ and a tail toward smaller separations. Thus, a significant fraction of PopIII binaries can form BBHs only via stable MT (see Fig. 7).

Fig. 9 shows the distribution of the coalescence time of PopIII BBHs. For the wide-binary model (red), the coalescence time distribution follows $dN/t_{\text{GW}} \propto t_{\text{GW}}^{-1}$ because of $\Gamma(a) \propto a^{-1}$. For the close-binary model, since the initial separation distribution is approximated as $\Gamma(a) \propto a^{\gamma}$ with $\gamma \gtrsim 0$ at $a \sim a_{\text{GW},0}$, the coalescence time distribution is approximated as $dN/dt_{\text{GW}} \propto t_{\text{GW}}^{-0.7+(\gamma-0.2)/4}$. Since most PopIII BBHs form at $z \simeq 10$, which corresponds to the cosmic age of $t_{\text{SF}} \simeq 1 \text{ Gyr}$, we require $10.8 \text{ Gyr} \lesssim t_{\text{GW}} + t_{\text{SF}} \lesssim 13.8 \text{ Gyr}$ for the PopIII BBHs to merge in the LIGO detection horizon ($0 \lesssim z \lesssim 0.2$, the corresponding time duration is $\sim 3 \text{ Gyr}$). From the distribution shown in Fig. 9, the fraction of merging PopIII BBHs detectable by LIGO (i.e., $9.8 \lesssim t_{\text{GW}}/\text{Gyr} \lesssim 12.8$) is estimated as $f_{\text{delay}} \simeq 0.17$ for both models and thus $f_{\text{BBH}} f_{\text{delay}} \simeq 1.7 \times 10^{-3}$ is obtained.

5 OBSERVATIONAL CONSTRAINTS ON POPIII BBH FORMATION SCENARIO

In this section, we discuss the possibility that PopIII stars can be the progenitors of the three BBH mergers detected by adLIGO, GW150914 (Abbott et al. 2016b), GW151226 and LVT151012 (Abbott et al. 2016d) based on the formation efficiencies obtained in the previous section and the total number of PopIII stars inferred from Planck’s result.

From the LIGO’s detections, the stellar-mass BBH merger rate is estimated as $\mathcal{R} \simeq 55_{-41}^{+99} \text{ Gpc}^{-3} \text{ yr}^{-1}$ (Abbott et al. 2016a). Assuming that the BH mass function of coalescing binaries follows

$$\Psi(M_1) \propto M_1^{-\alpha}, \quad (19)$$

with $M_{\text{min}} \leq M_2 \leq M_1$ and $M_1 + M_2 \leq 100 M_{\odot}$, and a uniform distribution on the secondary mass between $M_{\text{min}} = 5 M_{\odot}$ and M_1 , the power-law index is inferred as $\alpha \simeq 2.5_{-1.6}^{+1.5}$ (Abbott et al. 2016a).

Let us suppose that all the LIGO events originate from PopIII BBHs. We can evaluate the merger rate from the PopIII star formation rate as

$$\langle M_{\text{tot}} \rangle \mathcal{R} \simeq \dot{\rho}_{*,\text{III}} \frac{2f_{\text{bin}}}{1+f_{\text{bin}}} f_{\text{BBH}} f_{\text{delay}}, \quad (20)$$

where $\dot{\rho}_{*,\text{III}}$ is PopIII star formation rate (SFR), $f_{\text{bin}} (\simeq 0.7)$ is the binary fraction, f_{BBH} is the number fraction of merging BBHs within the Hubble time to the total number of PopIII stars, and f_{delay} is the number fraction of BBHs which merge in the LIGO detection horizon to the total number of merging PopIII BBHs. Here the mean mass of

BH masses is $\langle M_{\text{tot}} \rangle \simeq 30 M_{\odot}$ for $\alpha = 2.5$. Therefore the PopIII SFR required to explain all the LIGO events is

$$\dot{\rho}_{*,\text{III}} \simeq 1.3 \times 10^{-3} M_{\odot} \text{ yr}^{-1} \text{ Mpc}^{-3} \left(\frac{f_{\text{bin}}}{1+f_{\text{bin}}} / 0.4 \right)^{-1} \times \left(\frac{\langle M_{\text{tot}} \rangle}{30 M_{\odot}} \right) \left(\frac{\mathcal{R}}{60 \text{ Gpc}^{-3} \text{ yr}^{-1}} \right) \left(\frac{f_{\text{BBH}}}{0.01} \right)^{-1} \left(\frac{f_{\text{delay}}}{0.2} \right)^{-1}, \quad (21)$$

where we have used f_{BBH} obtained in §4, i.e., the efficiency of BBH formation only via stable MT, which we consider as the lower limit. For the two models for initial conditions of PopIII binaries, the number fraction of formed coalescing PopIII BBHs within the Hubble time is at least 1%, i.e., $f_{\text{BBH}} \gtrsim 0.01$. In this sense, the estimated PopIII SFR can be lower by a factor of a few. When we consider only GW150914, which has $\langle M_{\text{tot}} \rangle \simeq 65.3 M_{\odot}$ and $\mathcal{R} = 3.4_{-2.8}^{+8.6} \text{ Gpc}^{-3} \text{ yr}^{-1}$, the required PopIII SFR is $\dot{\rho}_{*,\text{III}} \simeq 0.15 \times 10^{-3} M_{\odot} \text{ yr}^{-1} \text{ Mpc}^{-3}$.

Now we compare directly the PopIII SFR of Eq. (21) with the constraint by the Planck measurement of the optical depth of the universe to electron scattering, which arises due to ionizing photons emitted from PopIII stars and other sources (e.g., accreting BHs). Thus, assuming that all the photons required to explain the observed optical depth are produced only by PopIII stars, the upper limit for the cumulative (comoving) mass density of PopIII stars is given by

$$\rho_{*,\text{III}} \lesssim 8.2 \times 10^5 M_{\odot} \text{ Mpc}^{-3} \times \left(\frac{\eta_{\text{ion}}}{5 \times 10^4} \right)^{-1} \left(\frac{f_{\text{esc}}}{0.1} \right)^{-1} \left(\frac{\tau_e - 0.066}{\Delta\tau_e} \right), \quad (22)$$

(Visbal et al. 2015; Inayoshi et al. 2016), where η_{ion} is the number of H-ionizing photons per stellar baryon, the escape fraction of ionizing photons from mini-haloes where PopIII stars form, and τ_e is the optical depth to electron scattering. The ionizing photon number per baryon is $\eta_{\text{ion}} = 7.1 (5.1) \times 10^4$ for the flat (Salpeter) IMF with a mass range of $10 \leq M/M_{\odot} \leq 100$ (Schaerer 2002). The value of the escape fraction $f_{\text{esc}} \simeq 0.1$ corresponds to dark-matter halos with masses of $> a \text{ few} \times 10^7 M_{\odot}$ (Wise et al. 2014), where most of the PopIII stars would form (see also Inayoshi et al. 2016). We here set our fiducial value to $\tau_e = 0.066 \pm \Delta\tau_e$, where $\Delta\tau_e = 0.016$ is the 1σ error (Ade et al. 2016). The PopIII SFR peaks at $z \simeq 10$ corresponding to the time scale of $\sim 0.5 \text{ Gyr}$ so that the upper bound of PopIII SFR is

$$\dot{\rho}_{*,\text{III}} \lesssim 1.3 \times 10^{-3} M_{\odot} \text{ yr}^{-1} \text{ Mpc}^{-3}. \quad (23)$$

This upper limit is consistent with the most probable value of the rate of all three events (see Eq. 21). Therefore we conclude that the PopIII BBH formation scenario can explain all the three BBH mergers detected in LIGO’s O1 run with the maximal PopIII formation efficiency inferred from the Planck measurement, even without BBHs formed by unstable MT or CE phases.

6 DISCUSSIONS

6.1 Gravitational wave background

A stochastic GW background (GWB) from unresolved PopIII BBH mergers is a useful probe for the existence of massive BBH populations at higher redshifts (Hartwig et al. 2016; Inayoshi et al. 2016; Dvorkin et al. 2016; Nakazato et al. 2016). Inayoshi et al. (2016) have estimated the amplitude of the PopIII GWB adopting a PopIII star-formation rate whose normalization is consistent with the Planck measurement of the electron scattering optical depth (see Eq 22). However, they also assume the merging rate of PopIII BBHs obtained by Kinugawa et al. (2014), which include BBHs formed by unstable MT and CE phases. According to the model by Kinugawa et al. (2014), 12 (2.6)% of PopIII binaries form BBHs coalescing within the Hubble time for the flat (Salpeter) IMF with $10 \leq M/M_\odot \leq 100$ and 37 (55)% of such BBHs (i.e., 4.2 (1.4)% of the total binaries) are formed without experiencing CE phases. On the other hand, the lower limit we estimate in §4 is only $\sim 1\%$ of total binaries. Therefore, the GWB amplitude produced by merging PopIII BBHs formed only by stable MT is several times smaller than that estimated by Inayoshi et al. (2016), but gives a lower limit of the GWB. The detectability of the PopIII GWB in the future observing run in Advanced LIGO/Virgo in five years depends on physical parameters relevant to reionization and high-redshift galaxies shown in Eq. (22).

6.2 Tidal force and stellar spins

In this paper, we neglect effects of stellar rotation on the evolution so far. As we discussed, non-rotating PopIII stars are likely to evolve to compact blue giants and thus can avoid unstable MT and CE phases during their lifetime. However, stellar rotation may change the evolution of Pop III stars because of hydrodynamical instabilities induced by rotation (e.g. meridional circulations). For a slow-rotating PopIII star with $v_{\text{rot}} \sim 0.2 v_{\text{Kep}}$ (v_{Kep} is the Keplerian velocity of the star), the effective temperature at the end of the main-sequence phase tends to be lower than for a non-rotating PopIII star with the same mass, because unburnt hydrogen is supplied to the core of the rotating PopIII star due to the mixing (Ekström et al. 2008; Takahashi et al. 2014). Furthermore, mixing of heavy elements would increase the opacity of the stellar envelope (Joggerst & Whalen 2011). Therefore, the rotating PopIII star tends to evolve to red giants instead of blue giants expected for the non-rotation case. Since a red giant has a bloated stellar convective envelope, the stellar radius is more likely to fill its Roche lobe and lead to unstable MT, which would result in CE phase. On the other hand, a fast-rotating PopIII star with $v_{\text{rot}} \gtrsim 0.5 v_{\text{Kep}}$, would experience chemically homogeneous evolution due to strong mixing effects and then become bluer without any redwards evolution (e.g. Yoon & Langer 2005; Woosley & Heger 2006; de Mink et al. 2009; Song et al. 2016). In this case, the PopIII stars can avoid unstable MT and CE phases.

The rotation period of a star in a close binary system is likely to be the same as the orbital period because of the tidal torque. This synchronization timescale of massive main sequence stars is estimated as (Kushnir et al. 2016a,b; see

also Zahn 1975):

$$t_{\text{tide}} \simeq 2 \text{ Myr } q^{-1/8} \left(\frac{1+q}{2q} \right)^{31/24} \left(\frac{r_g^2}{0.1} \right) \left(\frac{t_{\text{GW}}}{10 \text{ Gyr}} \right)^{17/8} \\ \times \left(\frac{R}{3 R_\odot} \right)^2 \left(\frac{R_{\text{con}}}{1.2 R_\odot} \right)^{-9} \left(\frac{M}{40 M_\odot} \right)^{109/24} \left(\frac{M_{\text{con}}}{24 M_\odot} \right)^{4/3}, \quad (24)$$

where R_{con} and M_{con} are the size and mass of the convective core, r_g^2 is the gyration radius of the star. Here the fiducial values are adopted from data calculated with the MESA code and approximate $\rho_{\text{con}}/\bar{\rho}_{\text{con}} \simeq 0.5$. PopIII main sequence stars in binaries are likely to be synchronized at orbital separations where the coalescence time is shorter than the Hubble time. Note that this estimate is very sensitive to the convective-core radius and the mass of the star.

Importantly, when they are tidally synchronized at the separation where the coalescence time corresponds to the Hubble time, the rotational velocity of synchronized PopIII main sequence stars is quite slow as $v_{\text{rot}} < (0.01 - 0.1) \times v_{\text{Kep}}$. Therefore, the stellar rotation does not play important roles irrespective with the initial spin. Of course, binaries with smaller separations, i.e., shorter coalescence times, the stellar rotation might play important roles. However, BBHs formed in such systems merge in the early universe and they are not observable by LIGO.

6.3 Remnants after common envelope phases

Throughout the paper, we do not discuss the outcome of PopIII binaries which experience CE phases, in order to give conservative arguments. Many previous studies concluded that possible outcomes after CE evolution are tight binaries and/or stellar mergers, but the bifurcation conditions are highly uncertain (e.g., Iben & Livio 1993; Taam & Sandquist 2000; Ivanova et al. 2013). Even for PopIII binaries, CE evolution would occur for massive stars with $M > 50 M_\odot$ because (1) the accretor expands due to violent MT from the donor or (2) the MT would be unstable when the donor has a deep convective envelope in the late stage of its evolution (see bottom panel in Fig. 7). If the CE evolution of such binaries does not lead to stellar mergers, possible types of the remnants would be binaries of a He star ($\gtrsim 20 M_\odot$) with a main-sequence star ($\gtrsim 40 M_\odot$) or a BH ($\gtrsim 30 M_\odot$) after the first/second episodes of MT. Subsequently, if any, they form massive BBHs coalescing due to GW emission within the Hubble time. In order to discuss the outcome after CE evolution of PopIII binaries, we need to understand basic properties of the stellar dynamics in the CE phases, e.g., the energy budget during the CE phases more precisely using stellar evolution calculations as studied for stars with $0.0004 \leq Z \leq 0.02$ (e.g., Kruckow et al. 2016).

7 SUMMARY

We study formation of stellar mass BBHs originating from PopIII stars, performing stellar evolution simulations for PopIII binaries with a public code MESA. We find that a significant fraction of PopIII binaries form massive BBHs through stable MT without experiencing CE phases. The formation efficiency of coalescing PopIII BBHs is estimated

for two different initial conditions for PopIII binaries with large and small separations, respectively. As a result, $\sim 10\%$ of the total PopIII binaries form BBHs only through stable MT and $\sim 10\%$ of these BBHs merge due to gravitational wave emission within the Hubble time. Furthermore, the chirp mass of merging BBHs has a flat distribution over $15 \lesssim M_{\text{chirp}}/M_{\odot} \lesssim 35$. This formation pathway of PopIII BBHs is presumably robust because stable MT is less uncertain than CE evolution, which is the main formation channel for PopII BBHs. We then test the hypothesis that the BBH mergers detected by LIGO originate from PopIII stars using our result and the upper limit on the total number of PopIII stars formed in the early universe as inferred from the optical depth measured by Planck. We conclude that the PopIII BBH formation scenario can explain the mass-weighted merger rate of the LIGO's O1 events with the maximal PopIII formation efficiency inferred from the Planck measurement, even without PopIII BBHs formed by unstable MT or CE phases.

ACKNOWLEDGEMENTS

We thank Georges Meynet for improving the paper as a referee. We also thank Zoltán Haiman, Takashi Hosokawa, Sylvia Ekström and Tilman Hartwig for useful discussions. This work is partially supported by the Simons Foundation through the Simons Society of Fellows (KI), Flatiron Fellowship (KH), by JSPS Research fellowship for young scientists (RH, No. 16J07613), and by JSPS KAKENHI Grant (TK, No. JP16818962).

REFERENCES

- Abbott B. P., et al., 2016a, *Physical Review X*, **6**, 041015
 Abbott B. P., et al., 2016b, *Physical Review Letters*, **116**, 061102
 Abbott B. P., et al., 2016c, *Physical Review Letters*, **116**, 131102
 Abbott B. P., et al., 2016d, *Physical Review Letters*, **116**, 241103
 Abbott B. P., et al., 2016e, *ApJ*, **818**, L22
 Abramowicz M. A., Czerny B., Lasota J. P., Szuszkiewicz E., 1988, *ApJ*, **332**, 646
 Ade P. A. R., et al., 2016, *A&A*, **594**, A13
 Baraffe I., Heger A., Woosley S. E., 2001, *ApJ*, **550**, 890
 Begelman M. C., 1978, *MNRAS*, **184**, 53
 Belczynski K., Bulik T., Rudak B., 2004, *ApJ*, **608**, L45
 Belczynski K., Kalogera V., Rasio F. A., Taam R. E., Zezas A., Bulik T., Maccarone T. J., Ivanova N., 2008, *ApJS*, **174**, 223
 Belczynski K., Ryu T., Perna R., Berti E., Tanaka T. L., Bulik T., 2016a, preprint, ([arXiv:1612.01524](https://arxiv.org/abs/1612.01524))
 Belczynski K., Holz D. E., Bulik T., O'Shaughnessy R., 2016b, *Nature*, **534**, 512
 Blandford R. D., Begelman M. C., 1999, *MNRAS*, **303**, L1
 Clark P. C., Glover S. C. O., Smith R. J., Greif T. H., Klessen R. S., Bromm V., 2011, *Science*, **331**, 1040
 Dominik M., Belczynski K., Fryer C., Holz D. E., Berti E., Bulik T., Mandel I., O'Shaughnessy R., 2012, *ApJ*, **759**, 52
 Dosopoulou F., Kalogera V., 2016a, *ApJ*, **825**, 70
 Dosopoulou F., Kalogera V., 2016b, *ApJ*, **825**, 71
 Dvorkin I., Vangioni E., Silk J., Uzan J.-P., Olive K. A., 2016, *MNRAS*, **461**, 3877
 Edwards D. A., Pringle J. E., 1987, *MNRAS*, **229**, 383
 Eggleton P. P., 1983, *ApJ*, **268**, 368
 Ekström S., Meynet G., Chiappini C., Hirschi R., Maeder A., 2008, *A&A*, **489**, 685
 Eldridge J. J., Stanway E. R., 2016, *MNRAS*, **462**, 3302
 Ge H., Hjellming M. S., Webbink R. F., Chen X., Han Z., 2010, *ApJ*, **717**, 724
 Ge H., Webbink R. F., Chen X., Han Z., 2015, *ApJ*, **812**, 40
 Greif T. H., Bromm V., Clark P. C., Glover S. C. O., Smith R. J., Klessen R. S., Yoshida N., Springel V., 2012, *MNRAS*, **424**, 399
 Hartwig T., Volonteri M., Bromm V., Klessen R. S., Barausse E., Magg M., Stacy A., 2016, *MNRAS*, **460**, L74
 Hayashi C., 1961, *PASJ*, **13**, 450
 Hayashi C., Hōshi R., Sugimoto D., 1962, *Progress of Theoretical Physics Supplement*, **22**, 1
 Hirano S., Hosokawa T., Yoshida N., Umeda H., Omukai K., Chikaki G., Yorke H. W., 2014, *ApJ*, **781**, 60
 Hjellming M. S., 1989, PhD thesis, Illinois Univ. at Urbana-Champaign, Savoy.
 Hjellming M. S., Webbink R. F., 1987, *ApJ*, **318**, 794
 Hosokawa T., Omukai K., Yoshida N., Yorke H. W., 2011, *Science*, **334**, 1250
 Hosokawa T., Omukai K., Yorke H. W., 2012, *ApJ*, **756**, 93
 Hosokawa T., Hirano S., Kuiper R., Yorke H. W., Omukai K., Yoshida N., 2016, *ApJ*, **824**, 119
 Hurley J. R., Tout C. A., Pols O. R., 2002, *MNRAS*, **329**, 897
 Iben Jr. I., Livio M., 1993, *PASP*, **105**, 1373
 Inayoshi K., Hosokawa T., Omukai K., 2013, *MNRAS*, **431**, 3036
 Inayoshi K., Kashiyama K., Visbal E., Haiman Z., 2016, *MNRAS*, **461**, 2722
 Ivanova N., et al., 2013, *A&ARv*, **21**, 59
 Jiang Y.-F., Stone J. M., Davis S. W., 2014, *ApJ*, **796**, 106
 Joggerst C. C., Whalen D. J., 2011, *ApJ*, **728**, 129
 Kinugawa T., Inayoshi K., Hotokezaka K., Nakauchi D., Nakamura T., 2014, *MNRAS*, **442**, 2963
 Kinugawa T., Nakamura T., Nakano H., 2016a, preprint, ([arXiv:1610.00305](https://arxiv.org/abs/1610.00305))
 Kinugawa T., Miyamoto A., Kanda N., Nakamura T., 2016b, *MNRAS*, **456**, 1093
 Kippenhahn R., Weigert A., 1990, *Stellar Structure and Evolution*
 Kolb U., Ritter H., 1990, *A&A*, **236**, 385
 Kruckow M. U., Tauris T. M., Langer N., Szécsi D., Marchant P., Podsiadlowski P., 2016, *A&A*, **596**, A58
 Kushnir D., Zaldarriaga M., Kollmeier J. A., Waldman R., 2016a, preprint, ([arXiv:1605.03810](https://arxiv.org/abs/1605.03810))
 Kushnir D., Zaldarriaga M., Kollmeier J. A., Waldman R., 2016b, *MNRAS*, **462**, 844
 Machida M. N., Omukai K., Matsumoto T., Inutsuka S.-i., 2008, *ApJ*, **677**, 813
 Mandel I., de Mink S. E., 2016, *MNRAS*,
 Mapelli M., 2016, *MNRAS*, **459**, 3432
 Marchant P., Langer N., Podsiadlowski P., Tauris T. M., Moriya T. J., 2016, *A&A*, **588**, A50
 Marigo P., Girardi L., Chiosi C., Wood P. R., 2001, *A&A*, **371**, 152
 Nakamura T., et al., 2016, *Progress of Theoretical and Experimental Physics*, **2016**, 093E01
 Nakazato K., Niino Y., Sago N., 2016, *ApJ*, **832**, 146
 O'Leary R. M., Meiron Y., Kocsis B., 2016, *ApJ*, **824**, L12
 Ohsuga K., Mori M., Nakamoto T., Mineshige S., 2005, *ApJ*, **628**, 368
 Omukai K., Palla F., 2003, *ApJ*, **589**, 677
 Omukai K., Tsuribe T., Schneider R., Ferrara A., 2005, *ApJ*, **626**, 627
 Paczyński B., 1967, *Acta Astron.*, **17**, 355
 Paczyński B., 1976, in Eggleton P., Mitton S., Whelan J., eds, IAU Symposium Vol. 73, *Structure and Evolution of Close Binary Systems*. p. 75
 Paczyński B., Sienkiewicz R., 1972, *Acta Astron.*, **22**, 73
 Pavlovskii K., Ivanova N., 2015, *MNRAS*, **449**, 4415

- Pavlovskii K., Ivanova N., Belczynski K., Van K. X., 2017, *MNRAS*, **465**, 2092
- Paxton B., Bildsten L., Dotter A., Herwig F., Lesaffre P., Timmes F., 2011, *ApJS*, **192**, 3
- Paxton B., et al., 2013, *ApJS*, **208**, 4
- Paxton B., et al., 2015, *ApJS*, **220**, 15
- Portegies Zwart S. F., McMillan S. L. W., 2000, *ApJ*, **528**, L17
- Rodriguez C. L., Chatterjee S., Rasio F. A., 2016, *Phys. Rev. D*, **93**, 084029
- Ryu T., Tanaka T. L., Perna R., 2016, *MNRAS*, **456**, 223
- Savonije G. J., 1978, *A&A*, **62**, 317
- Sądowski A., Narayan R., Tchekhovskoy A., Abarca D., Zhu Y., McKinney J. C., 2015, *MNRAS*, **447**, 49
- Schaerer D., 2002, *A&A*, **382**, 28
- Soberman G. E., Phinney E. S., van den Heuvel E. P. J., 1997, *A&A*, **327**, 620
- Song H. F., Meynet G., Maeder A., Ekström S., Eggenberger P., 2016, *A&A*, **585**, A120
- Stacy A., Bromm V., 2013, *MNRAS*, **433**, 1094
- Stacy A., Greif T. H., Bromm V., 2012, *MNRAS*, **422**, 290
- Stacy A., Bromm V., Lee A. T., 2016, *MNRAS*, **462**, 1307
- Susa H., Hasegawa K., Tominaga N., 2014, *ApJ*, **792**, 32
- Taam R. E., Sandquist E. L., 2000, *ARA&A*, **38**, 113
- Takahashi K., Umeda H., Yoshida T., 2014, *ApJ*, **794**, 40
- Tout C. A., Aarseth S. J., Pols O. R., Eggleton P. P., 1997, *MNRAS*, **291**, 732
- Turk M. J., Abel T., O’Shea B., 2009, *Science*, **325**, 601
- Visbal E., Haiman Z., Bryan G. L., 2015, *MNRAS*, **453**, 4456
- Wise J. H., Demchenko V. G., Halicsek M. T., Norman M. L., Turk M. J., Abel T., Smith B. D., 2014, *MNRAS*, **442**, 2560
- Woolley S. E., Heger A., 2006, *ApJ*, **637**, 914
- Yoon S.-C., Langer N., 2005, *A&A*, **443**, 643
- Zahn J.-P., 1975, *A&A*, **41**, 329
- de Mink S. E., Cantiello M., Langer N., Pols O. R., Brott I., Yoon S.-C., 2009, *A&A*, **497**, 243

APPENDIX A: NON-CONSERVATIVE MASS TRANSFER: THE DEPENDENCE ON β

Through the paper, we set the value of β , which is a parameter to describe the efficiency of non-conservative mass transfer. We adopt $\beta = 0.1$ as our fiducial value. In this appendix, we briefly discuss the dependence of the choice of β on the results. The orbital evolution is described by Eq. (3). Integrating this equation over the second episode of MT, where the donor is a star with M_1 and the accretor is a BH with M_2 , the orbital separation after the MT is given by

$$a_f = \left(\frac{M_{1i}}{M_{1f}} \right)^2 \left(\frac{M_{2i}}{M_{2f}} \right)^{2/\beta} \left(\frac{M_{1i} + M_{2i}}{M_{1f} + M_{2f}} \right) a_i, \quad (\text{A1})$$

where the subscript i and f indicate the values before and after the MT, respectively, and $M_{2f} = M_{2i} + \beta(M_{1i} - M_{1f})$. For $\beta = 0$, M_2 does not change via the MT, we obtain

$$a_f = \left(\frac{M_{1i}}{M_{1f}} \right)^2 \left(\frac{M_{1i} + M_2}{M_{1f} + M_2} \right) e^{2(q_{1f} - q_{1i})} a_i. \quad (\text{A2})$$

Fig. A1 presents the time evolution of the orbital separation and the BH mass with the same initial conditions as shown in Figs. 3 and 5 for different values of β . For $\beta \lesssim 0.1$, the resultant track of the separation and the BH (accretor) mass do not change significantly since the final separation can be written by Eq. (A2) for smaller β . For conservative MT ($\beta = 1$), the final orbital separation is similar to those for $\beta \lesssim 0.1$, but the BH mass becomes higher. However, a

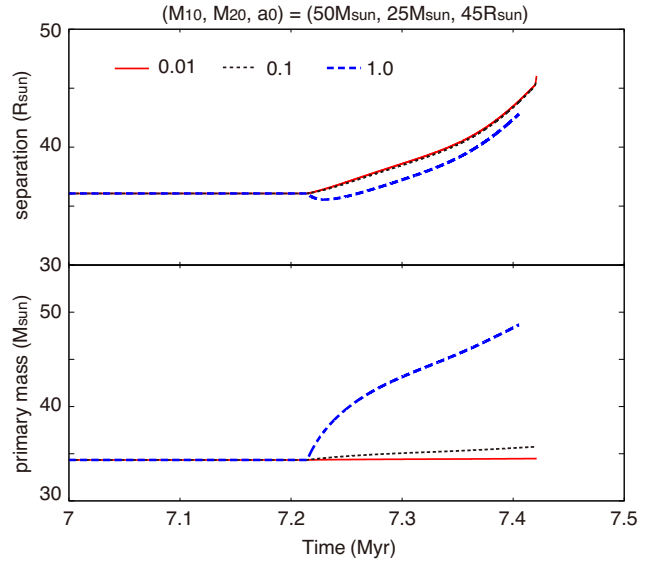


Figure A1. Time evolution of the orbital separation and the BH (accretor) with initial conditions of $M_{1,0} = 50 M_{\odot}$, $M_{2,0} = 25 M_{\odot}$ and $a_0 = 45 R_{\odot}$ for different values of β , which describes the efficiency of non-conservative mass transfer.

significant fraction of the transferred mass would be ejected from the system because the accretion flow onto the BH releases a huge amount of energy as radiation and/or outflows (e.g. Blandford & Begelman 1999; Ohsuga et al. 2005; Jiang et al. 2014; Sądowski et al. 2015).